NaumovStanislav@yandex.ru

Russian-Chinese Symposium 2023

Naumov S., Panov D., Belinin D., Sokolovsky V., Volokitina E., Salishchev G.

Structure and mechanical properties of Ti_2AlNb-based joints produced by gas tungsten arc welding and others

Nowadays, plasma, gas tungsten arc welding, laser, diffusion, and electric resistance welding of Ti_2AlNb-based alloys attract greatest interest. Various techniques for welding of such alloys are considered and proposed in the work. A defect-free weld with an optimal structure is formed due to the high welding speed and the concentration of thermal energy or the absence of the need to melt the metal. The welding modes are selected and the technological features of plasma, laser, diffusion, and electric resistance welding with obtaining the optimal structural state and strength properties up to 90% of the base metal.

Laser Welding Technology

1. Laser beam welding

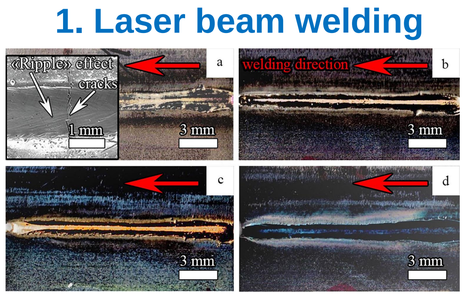

Figure - 3. Appearance of welds obtained at: a) room temperature; b) preheating 400 °C; c) 600 °C; d) 800 °C. The red arrows indicate the direction of the laser beam welding

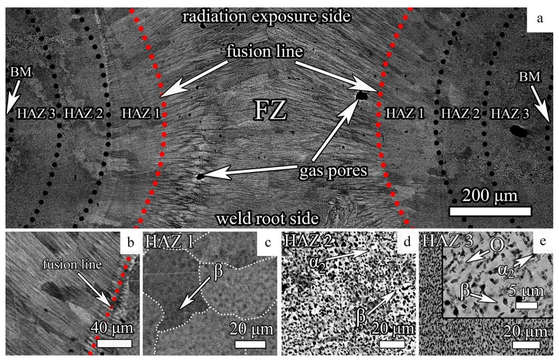

Figure - 4. Transverse structure of the weld after LBW at room temperature: a) macrostructure; b) FZ; c) HAZ1; d) HAZ2 e) HAZ3

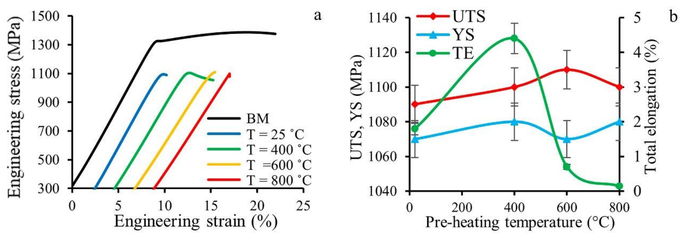

Figure – 5. Mechanical properties of welded joints obtained by LBW: a) stress-strain curves of the initial state and welded joints; b) dependence of properties on preheating temperature

2. Pulsed laser beam welding

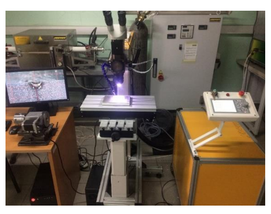

Figure - 6. Equipment for laser welding of the LAT-S-300 series

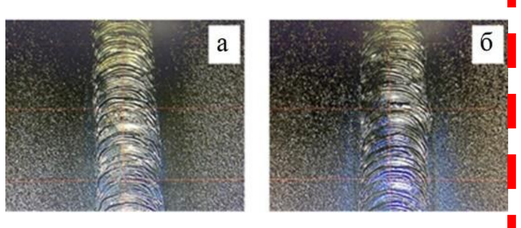

Figure - 7. Appearance of the welded joint depending on the voltage and pulse duration: a) 280 V, 6 ms; б) 300 V, 6 ms

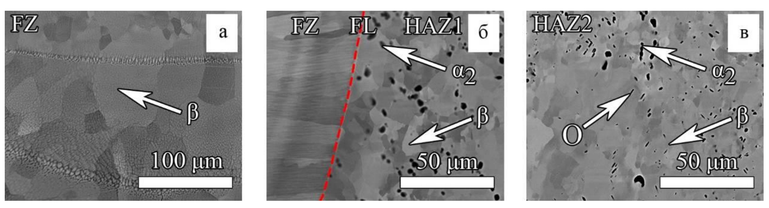

Figure - 8. Zones of the Ti_2AlNb welded joint obtained by PLBW at 300 V, 6 ms modes: a) melting zone (FZ); б) fusion line (FL) and first heat affected zone (HAZ1); в) second heat affected zone (HAZ2)

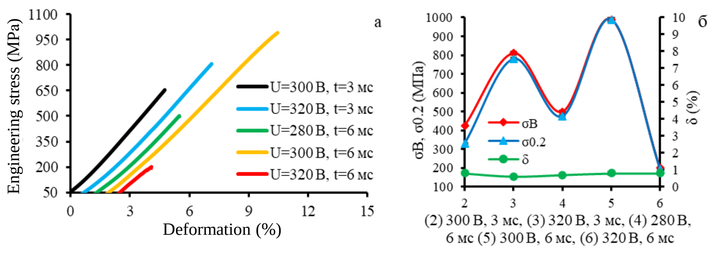

Figure - 9. Mechanical properties of welded joints: a) tensile diagram; б) graph of the mechanical properties of the welded joint depending on the modes of PLBW

Plasma Welding Technology

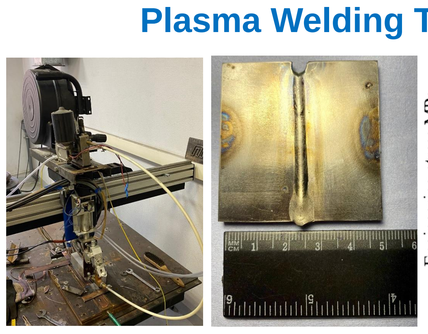

Figure - 10. Plasma welding equipment and the appearance of the welded joint

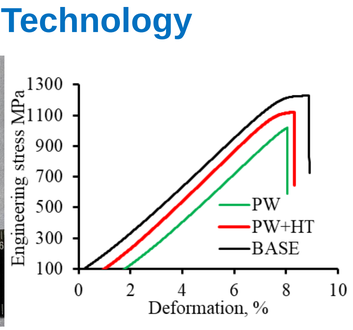

Figure - 11. Mechanical properties of welded joints

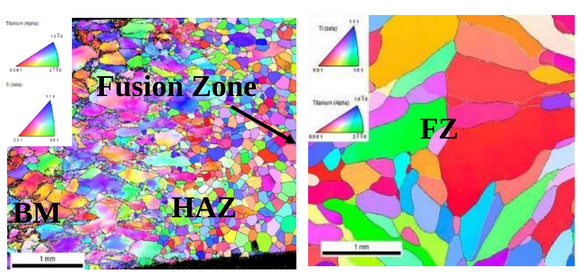

Figure – 12. EBSD-maps of welded joints in the cross-section of the weld

Ti_2AlNb alloy

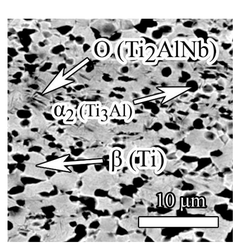

Figure - 1. Microstructure of the program Ti_2AlNb alloy in the initial condition: (a) BSE-SEM and (b) bright field TEM images

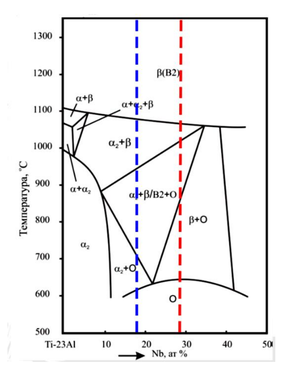

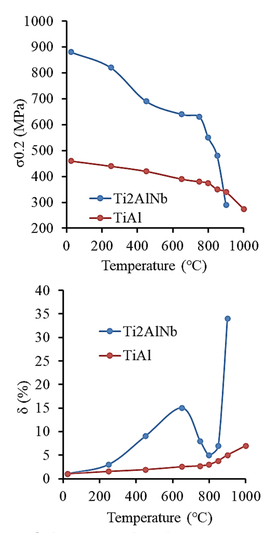

Figure - 2. Diagram of alloys of the Ti-Al-Nb system and dependence of properties on temperature

VTI-4 alloy was used in this work (Ti-23Al-23Nb-1.4V-0.8Zr-0.4Mo-0.4Si at. %). Gas tungsten arc welding of an alloy VTI-4 based on orthorhombic titanium aluminide (Ti_2AlNb) was studied (Fig. 13-16). Elongated large dendrites and globular β-grains were found in the center and the root part of the weld, respectively. The formation of such a structure was associated with slower solidification of the weld surface, while, in the root part of the weld, there was a rapid heat removal due to heat exchange and additional cooling by shielding gas supply. Meanwhile, the strength level of welded joints of the alloy under study was ≈ 90 % of the base metal at pulse welding mode (σ_B = 1100 MPa, $\sigma_{0.2}$ = 1030 MPa, δ = 1.1 %, 340-380 $HV_{0.2}$).

Factors affecting weldability:
composition, ↑ elastic stresses due to a cascade of phase transformations during the crystallization of the melt and cooling of the heat affected zone, ↓ plasticity, ↓ thermal conductivity

Factors affecting the quality of the joint:
thickness to be welded, quality of protection (gas, vacuum), welding parameters, preheating and postheating, heat treatment after welding

GTAW

No.	Current, A	Pulse frequency, Hz	
1	80-85	-	Local lack of fusion
2	150-155	-	Burn-through
3	110-115	-	-
4	80-85	2	Low frequency
5	80-85	>100	High frequency
6	110-115	>100	High frequency

Figure - 13. TIG-welding equipment and GTAW modes of VTI-4 alloy plates, blowing gas and gas to burner = 15 l/min

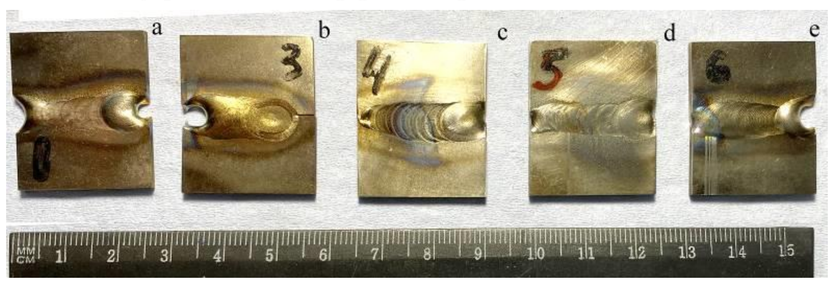

Figure – 14. Appearance of welds obtained by GTAW at different modes: (a) No.1; (b) No.3; (c) No.4; (d) No.5; (e) No.6

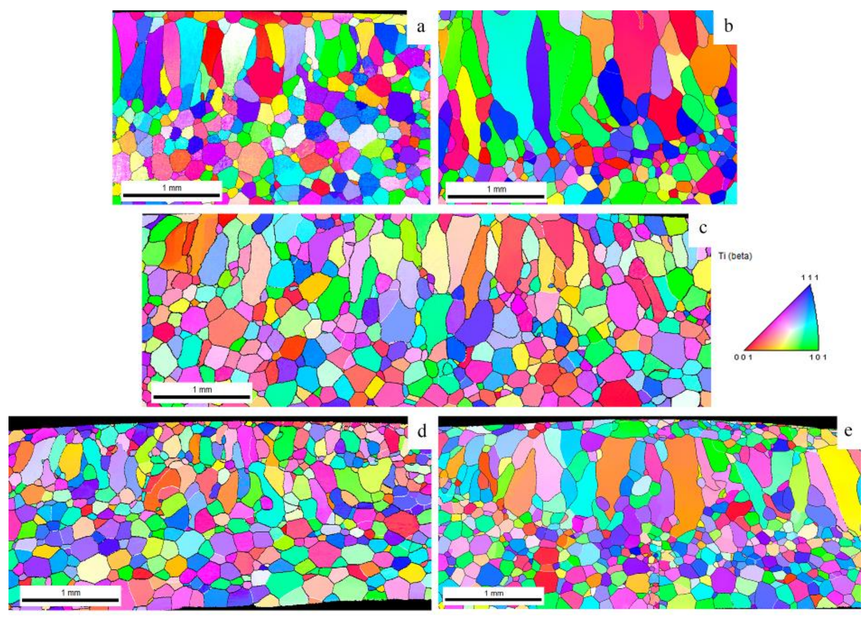

Figure – 15. EBSD-maps of welded joints in the cross-section of the weld depending on the GTAW modes: (a) No.1; (b) No.3; (c) No.4; (d) No.5; (e) No.6

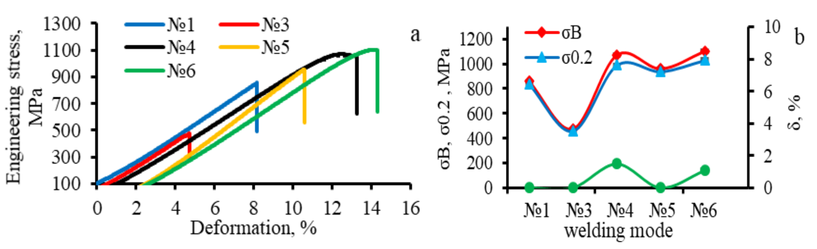

Figure - 16. Tensile graph of welded joints obtained by TIG-welding: 1-2 forced currents; 3 low frequency pulse current; 4-7 high frequency pulse current

Diffusion welding technology

1. Diffusion welding

Figure - 17. Equipment SPS 10-3 for diffusion welding in vacuum (10^{-4} Torr)

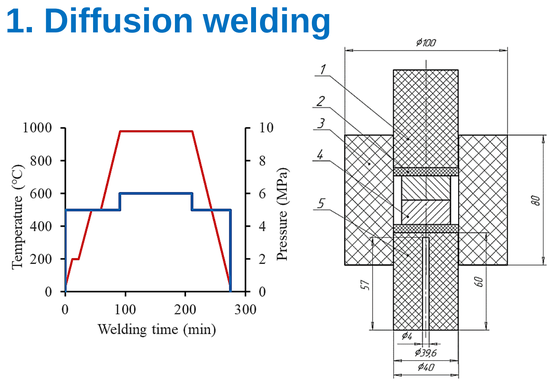

Figure - 18. Welding cyclogram and image of the placement of samples inside the matrix with punches: 1 - upper punch; 2 - corundum electrically insulating plate; 3 - matrix; 4 - welded samples; 5 lower punch with a technological hole for a thermocouple

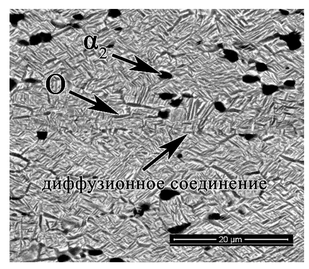

Figure - 19. Microstructure of the diffusion bonding of an alloy based on Ti_2AlNb, x5000

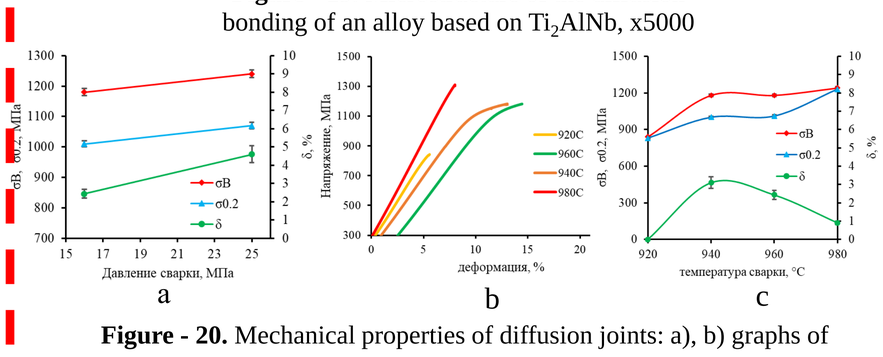

Figure - 20. Mechanical properties of diffusion joints: a), b) graphs of the mechanical properties of diffusion joints depending on the welding temperature; c) mechanical properties of the diffusion joint at a temperature of 960 °C depending on the welding pressure

2. Electric resistance welding

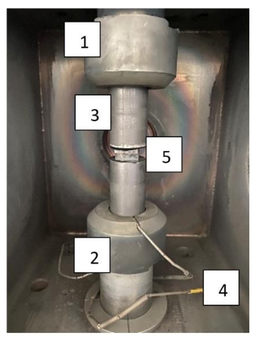

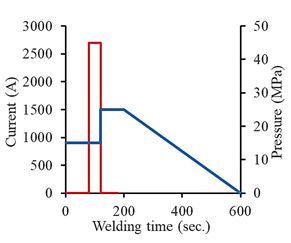

Figure - 21. Welding cyclogram and image of the placement of samples: 1 - hydraulic cylinder, 2 - graphite insert, 3 - punches, 4 - thermocouple, 5 - welded blanks

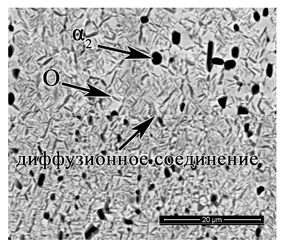

Figure - 22. Microstructure of the diffusion bonding of an alloy based on Ti_2AlNb, x5000

Electron Beam Welding

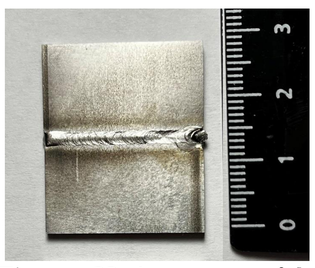

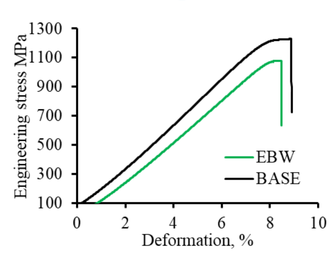

Figure - 23. Appearance of the welded joint obtained by EBW and tensile graph of welded joints

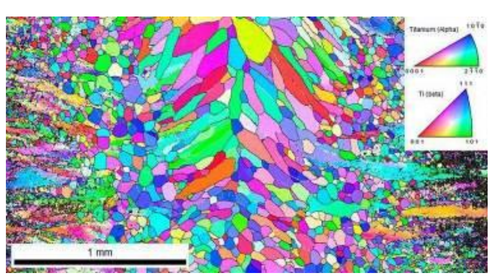

Figure – 24. EBSD-maps of welded joints in the cross-section of the weld

The authors gratefully acknowledge the financial support from the Russian Science Foundation Grant № 19-79-30066. The authors are grateful to the personnel of the Joint Research Center, «Technology and Materials», Belgorod State National Research University, for their assistance with the instrumental analysis.